materials

MDPI

Article

Low-Frequency Bandgap Study of Phononic Crystal Double-Layer Beams Based on Spatial Positive Quadrilateral Localised Oscillators

Haoyun Zhou, Qiming Liu and Denghui Qian *

School of Naval Architecture & Ocean Engineering, Jiangsu University of Science and Technology, Zhenjiang 212100, China
* Correspondence: dhqian@just.edu.cn

Abstract

A phononic crystal double-layer beam incorporating spatial ortho-quadrilateral local oscillators was investigated for low-frequency vibration attenuation. This structure was based on the periodic arrangement of oscillators in space, constructing a double-layer beam structure of phononic crystal with local oscillators based on spatial regular quadrilateral arrangements. The energy band structure, transmission curve, and displacement field corresponding to characteristic modes of this structure were calculated using the finite element software COMSOL 6.2, and research was conducted on the bandgap characteristics of the structure. The bandgap characteristics of two configurations were investigated: a single-layer structure consisting of one longitudinal steel beam coupled to local oscillators, and a double-layer structure consisting of two parallel steel beams connected through these oscillators. Adjustable parameters can achieve fixed vibration control in the low-frequency range.

Keywords: phononic crystals; vibration attenuation; bandgap characteristics; the structure of the band; displacement field

1. Introduction

Vibration and noise control are important issues in ship structures and other engineering applications. Excessive structural vibration can induce resonance and fatigue damage, reduce the accuracy of precision instruments, and affect the operational stability and service life of onboard equipment. Meanwhile, prolonged exposure to high noise levels may cause hearing impairment, sleep disturbances, and other adverse effects on human health. In civil marine applications, vibration generated by ship machinery and propulsion systems can also contribute to underwater noise, which may interfere with the communication, navigation, and behaviour of marine fauna. Therefore, effective vibration control is important not only for improving the safety and operational performance of ships but also for reducing potential environmental impacts and protecting marine ecosystems. Traditional ship vibration damping materials are less effective, and cannot be specific to frequency vibration damping, while the phononic crystal is a periodic elastic material and has the characteristics of the elastic bandgap composite structure materials, can be in a specific band of vibration blocking, and can make up for the shortcomings of the traditional materials. Beam structures are widely used in engineering applications due to their high strength and structural stability. In this study, beam structures refer to longitudinal steel beams coupled with periodically arranged local oscillators, including single-layer and double-layer configurations. As illustrated in Figure 1c–e, the double-layer structure consists of two

Check for updates

Academic Editor: Michael M. Sigalas

Received: 29 October 2026
Revised: 17 November 2026
Accepted: 20 November 2026
Published: 23 November 2026

Copyright: © 2026 by the authors. Licensee MDPI, Basel, Switzerland. This article is an open access article distributed under the terms and conditions of the Creative Commons Attribution (CC BY) license.

parallel steel beams connected through local oscillators. Introducing phononic crystal concepts [1] into such beam structures [2–4] may provide an effective approach for attenuating structural vibrations in selected frequency ranges. Phononic crystals have been extensively investigated for elastic wave control and vibration attenuation. Kushwaha et al. [5] studied the acoustic band structures of periodic elastic composites, while Martínez-Sala et al. [6] experimentally observed sound attenuation in a periodic structure. Subsequently, Laude et al. [7] investigated evanescent Bloch waves and complex band structures, providing further insights into wave attenuation mechanisms. More recently, Röhlig et al. [8] introduced function phononic crystals with spatially continuous material parameters, and further demonstrated the formation of giant acoustic bandgaps in phononic crystals with touching solid inclusions [9]. Röhlig and Laude [10] further investigated the influence of constriction geometry on the formation of wide bandgaps in artificial crystals. hence studies provide important theoretical and experimental foundations for the development of periodic structures for vibration and wave control.

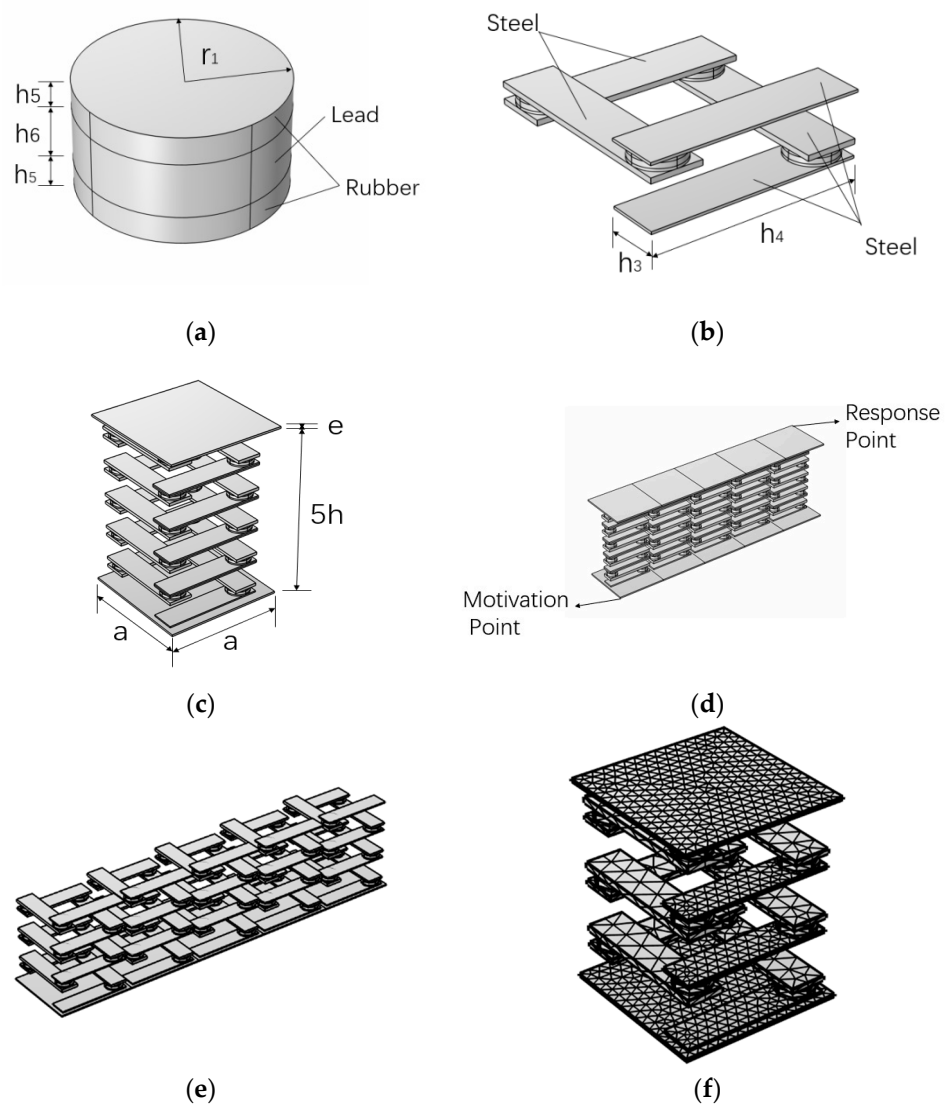

Figure 1. Model diagrams of the phononic crystal beam structures with ortho-quadrilateral local oscillators: (**a**) rubber–lead–rubber composite element; (**b**) ortho-quadrilateral local oscillator; (**c**) double-layer beam unit cell; (**d**) double-layer beam structure; (**e**) single-layer beam structure; (**f**) finite element mesh of the double-layer beam unit cell.

Phononic crystals are based on the concept of photonic crystals, which are periodic structures composed of two or more elastic materials that control vibration by suppressing the propagation of elastic waves. In the existing research on phononic crystals, there are mainly two types of bandgap formation mechanisms, one is Bragg scattering type, and the other is local-resonance type, in which the lattice constant of the former belongs to one order of magnitude to the corresponding bandgap frequency wavelength, while the lattice constant of the latter is much smaller than the corresponding bandgap frequency wavelength.

As phononic crystals were further developed, the study of them became more refined. Chen et al. [11] proposed a multi-objective optimisation method using radial basis function neural network and finite element method to model the algorithm, and NSGA-II algorithm to find the optimal solution, and the optimisation results show that the bandgap width and the attenuation depth are significantly increased. Jiang et al. [12] proposed a folded piezoelectric-phononic crystal beam model, which can realise Bragg and local-resonance bandgap at the same time, and obtain a strong attenuation characteristics of low frequency and high frequency. Xiao et al. [13–18] proposed a new local-resonance phononic crystal plate design, which consists of a homogeneous thin plate with "double cantilever beam" structures periodically arranged along the two-dimensional space. Wu et al. and Pennec et al. [19] designed and analysed a locally resonant phononic crystal plate structure consisting of periodically arranged cylinders attached to a homogeneous thin plate, and showed that a locally resonant full bandgap can be generated in this structure. Zhang et al. [20] designed a spiral-type phononic crystal structure for low-frequency sound insulation of high-speed trains, which produced a bending wave bandgap in the range of 108 to 153 Hz. Kang et al. [21] designed a phononic crystal plate consisting of a hollow lead column coated with a silicone rubber coating and connected with a short epoxy resin plate, and showed that it produced a bandgap with a width of 420 Hz. Zhang et al. [22] proposed a locally resonant pentagonal phononic crystal beam structure consisting of steel connecting plates and rubber–lead–rubber composite elements. By combining finite element analysis with Bloch–Floquet periodic conditions, they investigated the energy band structure, transmission attenuation characteristics, and vibration modes of the proposed structure. Their results showed that the pentagonal local resonator exhibited two bandgaps at 60–70 Hz and 107–130 Hz. Furthermore, the double-layer beam structure demonstrated more pronounced vibration attenuation than the corresponding single-layer beam. This study provided an important reference for the design of spatially arranged locally resonant phononic crystal beams. Nevertheless, the influence of alternative spatial resonator configurations on the low-frequency bandgap characteristics warrants further investigation.

In order to further investigate the damping effect of the phononic crystal beam structure [23], especially to improve its damping performance in the low-frequency range, in this paper, according to the periodic arrangement of the crystal cell structure in the space, the method of nesting the periodic structure with the periodic structure [24,25] is utilised to construct the phononic crystal double-layer beam structure with the spatial positive tetragonal local oscillator, which is designed to have a lower bandgap starting point and a wider forbidden band range compared with the conventional phononic crystal structure, which can open a lower bandgap starting point and a wider forbidden band range at low frequencies. To further investigate the influence of spatial resonator configurations on the low-frequency vibration attenuation characteristics of phononic crystal beams, a locally resonant quadrilateral configuration is proposed in this study. Unlike the previously reported pentagonal resonator [22], the proposed quadrilateral resonator consists of five steel connecting plates connected by four rubber–lead–rubber composite elements, resulting in a different spatial arrangement and connectivity of the resonator components. Placidi

et al. [26] experimentally investigated the existence of frequency bandgaps in microstructured materials, providing experimental evidence for vibration attenuation in periodic structures. In addition, Boutin et al. [27] investigated the mechanical behaviour of elastic crenelated beams using homogenisation methods, demonstrating the influence of periodic microstructures and local deformation on the effective mechanical response of beam structures. These studies provide useful references for understanding the bandgap characteristics and vibration attenuation behaviour of phononic crystal beam structures.

The energy band structures, transmission characteristics, and vibration modes of the quadrilateral and two-sided resonator configurations are investigated using the finite element method in COMSOL 6.2 Multiphysics. Subsequently, the vibration attenuation characteristics of single-layer and double-layer beam structures are analysed, and the effects of key geometric parameters are examined. The main contribution of this study lies in investigating an alternative spatial resonator configuration and clarifying its low-frequency bandgap and vibration attenuation characteristics within the established double-layer beam framework.

2. Modelling and Methodology

The model structure of the ortho-quadrilateral local vibrator developed in this paper in accordance with the local-resonance mechanism is shown in Figure 1b. Here, the term "ortho-quadrilateral" refers to the spatial arrangement of the connecting plates and composite elements in the local oscillator, as illustrated in Figure 1b. The corresponding single-layer and double-layer beam structures are shown in Figure 1d–e. The double-layer beam structure consists of five double-layer beam cells arranged periodically in the transverse direction, and the double-layer beam cells are composed of the upper and lower steel beams as well as the ortho-quadrilateral vibrators placed vertically and uniformly between the beams, and the ortho-quadrilateral vibrators are composed of five steel connecting plates and four multilayered cylindrical flats connected sequentially, and the multilayered cylindrical flats are composed of the material of "rubber-lead-rubber" as shown in Figure 1a. The multilayer cylindrical flat plate is made of "rubber-lead-rubber" material as shown in Figure 1a, and the connecting plates are connected to the neighbouring multilayer cylindrical flat plates sequentially according to the orientation of the square in the space. The double-layer beam single-cell structure as well as the double-layer beam structure are shown in Figure 1c,d. The lattice constants of the double-layer beam structure, the thickness of the upper and lower beams, the thickness of the thin plates connected in the oscillator, the thickness of the thick plates connected in the oscillator, the width and the length of the connected plates, the thickness of the rubber layer, the thickness of the lead layer, the height of the single local oscillator, and the radii of the multilayer cylinders are a, e, h1, h2, h3, h4, h5, h6, h, and r1, respectively. The material parameters for the orthogonal quadrilateral double-layer beam structure and geometrical parameters are shown in Tables 1 and 2.

Table 1. Material parameters used in the calculations.

Material	Density/(kg·m^{-3})	Poisson's Ratio	Young's Modulus × 10^{10}/(N·m^{-2})
steel	7780	0.300	21.060
Lead	11,600	0.369	4.080
Rubber	1300	0.469	1.175 × 10^{-5}

Table 2. Geometrical parameters used in the calculation of orthogonal double-layer beams units (mm).

Parameter	*a*	*e*	*h1*	*h2*	*h3*	*h4*	*h5*	*h6*	*h*	*r1*
Numerical value	110	1.5	1.5	3	24	100	2	4	36	12

In order to compare the damping characteristics of the phononic crystal bilayer beam structure with ortho-tetragonal local oscillators, a phononic crystal bilayer beam structure with ortho-tetragonal (ortho-tetragonal does not exist in the space and is named so in order to keep the name consistent with ortho-tetragonal) local oscillators has been constructed. The multilayer cylinder, local oscillator, double-layer beam single cell, and double-layer beam structure of this double-layer beam structure are shown in Figure 2a–d. The orthotropic bilayer beams are constructed in the same manner as the orthotropic tetragonal bilayer beams where the lattice constants of the orthotropic bilayer beams, the thicknesses of the upper and lower beams, the thicknesses of the connecting thin plates in the oscillator, the thicknesses of the connecting thin plates in the oscillator, the widths and lengths of the connecting plates, the thicknesses of the rubber layer, the thicknesses of the lead layer, the heights of the individual localised oscillators as well as the radiuses of the multilayer cylinders are *a, E, H1, H2, H3, H4, H5, H6, H,* and *R1*. The material and geometrical parameters of the orthotropic double-layer beam structure are shown in Tables 1 and 3. The height of the oscillator, the total height and the other parameters of the material are controlled to be the same for both the orthotropic and quadrilateral double-layer beams and the bandgap characteristics are compared by calculating the energy band structure and the transmission curves of both the beams.

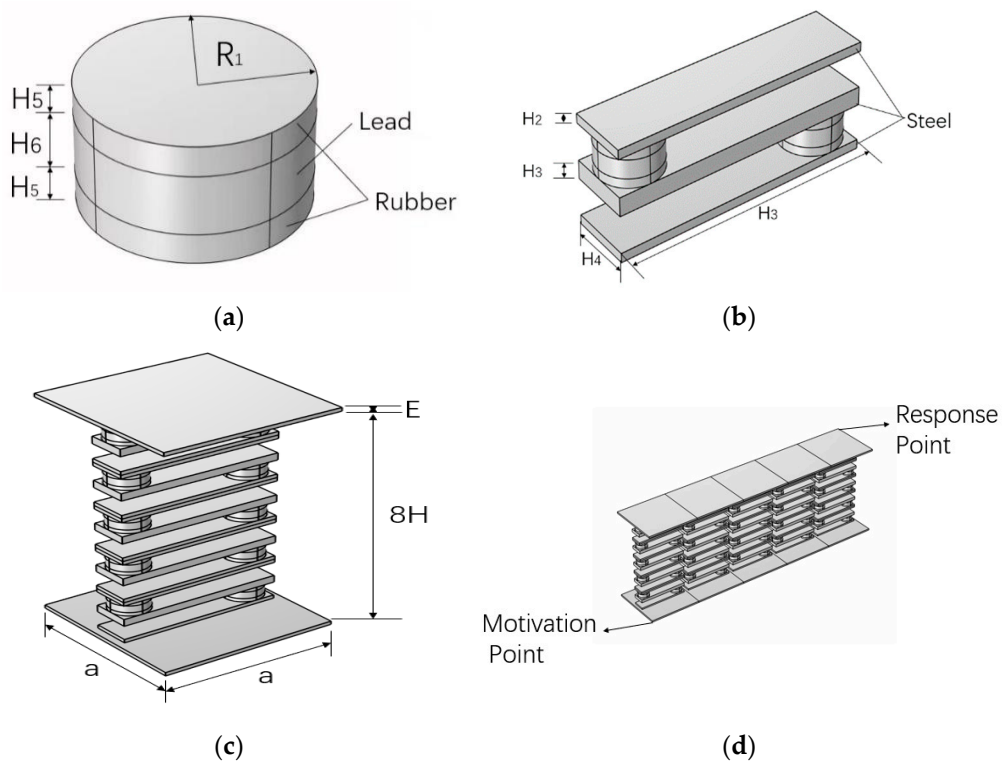

Figure 2. Schematic diagrams of the phononic crystal double-layer beam with the reference local oscillator configuration: (**a**) rubber–lead–rubber multilayer cylindrical element; (**b**) local oscillator assembly consisting of steel connecting plates and multilayer cylindrical elements; (**c**) double-layer beam unit cell; (**d**) finite double-layer beam structure showing the excitation and response points.

Table 3. Geometrical parameters used in the calculation of orthotropic double-layered beam units (mm).

Parameter	*a*	*E*	*H1*	*H2*	*H3*	*H4*	*H5*	*H6*	*H*	*R1*
Numerical value	110	1.5	3	6	24	100	2	4	36	12

In the above-described orthogonal and bipartite single-cell structures, the thickness of the upper and lower connecting plates is half of the thickness of the connecting plate in the middle portion, and due to the uniform placement of the local field oscillators between the upper and lower layers of the beams in the vertical direction, the thickness of the lower connecting plate of the local field oscillator arranged above and the upper connecting plate of the local field oscillator arranged above bonded together is exactly that of the intermediate connecting plate, which strengthens the periodicity of the double-layer beam structure in the vertical direction. The periodic unfolding of the double-layer beam singlet structure in the longitudinal direction constitutes the phononic crystal double-layer beam structure, which enhances the two-dimensional periodicity of the double-layer beam structure through the periodic unfolding of the local field oscillator in the transverse direction and the periodic unfolding of the double-layer beam singlet in the longitudinal direction, and the double-layer beam structure is strengthened by the way of the periodic structures nesting with each other, which enables this kind of double-layer beam structure to open up the wider forbidden band at the low frequency.

The transmission matrix method [28], plane wave expansion method [29], multiple scattering method [30], and finite element method are the main computational methods used at this stage to study the computational properties of elastic wave bandgap. In this paper, we mainly use the finite element method, based on the commercial software COMSOL Mutiphysics to simulate the bandgap of the ortho-quadrilateral as well as ortho-bipartite model to bring out the energy band structure diagram, and compare the band-structure predictions with the transmission responses of finite periodic structures. In this paper, the models were meshed using a physics-controlled mesh in COMSOL Multiphysics. Taking the ortho-quadrilateral local oscillator double-layer beam unit cell as an example, the mesh consists of 8023 tetrahedral elements, and quadratic serendipity shape functions were adopted for displacement interpolation. Similar meshing strategies were employed for the other models. The calculated results showed only minor variations with mesh refinement, indicating low sensitivity to mesh density. All materials were assumed to be linearly elastic, and material damping was neglected in the numerical simulations. The periodic boundary condition derived from the Bloch–Floquet theorem is used for the intersection interface of adjacent vibrators,

$$u(z + a) = u(z) \cdot e^{i(k \cdot a)} \tag{1}$$

Substituting the periodic boundary condition Equation (1) into the finite element eigenequation of the free vibration, we can obtain

$$Ku = w^2 Mu \tag{2}$$

where the stiffness matrix K and the mass matrix M are both contained. In this equation, the stiffness matrix K and mass matrix M contain coupled Bloch wavevector terms, which are different from the stiffness and mass matrices in the conventional finite element characteristic equation. Equation (2) is a typical generalised eigenvalue problem with respect to ω^2. For each given Bloch wavevector k, a corresponding series of eigenfrequencies can be obtained by solving for the eigenvalues. The eigenfrequency problem was solved in COMSOL Multiphysics using a parametric sweep of the Bloch wave vectors, with N = 50. Bloch–Floquet periodic conditions were applied to the corresponding periodic boundaries, while the remaining external boundaries were treated as free boundaries. By traversing all the wave vectors on the boundary of the irreducible Brillouin zone, the energy band structure of the oscillator is finally obtained. Unlike the finite-difference time-domain (FDTD) method, which typically calculates wave propagation through time stepping, the present approach employs the finite element method (FEM) implemented in COMSOL Multiphysics to directly solve the eigenfrequency problem for prescribed Bloch wave vectors. This approach

is suitable for modelling complex three-dimensional geometries and material interfaces. The present analysis focuses on the dispersion characteristics of ideal periodic structures, while the vibration attenuation of finite structures is evaluated separately through displacement transmission responses. Acoustic radiation and fluid–structure interactions are not considered. The Bloch–Floquet periodicity condition is set between neighbouring vibrators to simulate a transverse infinite periodic connection, and the displacement transmission level is calculated using

$$T = 20\log_{10}\left(\frac{|u_{\text{out}}|}{|u_{\text{in}}|}\right) \quad (3)$$

where T denotes the displacement transmission level in decibels, and u_in and u_out represent the displacement amplitudes at the excitation and response points, respectively. Negative values of T indicate vibration attenuation, with more negative values corresponding to stronger attenuation.

Wu Xudong et al. found that the number of cycles of the vibrator has an important influence on the bandgap, the more cycles the better the bandgap effect. However, in practice, the structure should meet the requirements of lightweight and flexibility, and the structure should be as small as possible while meeting the vibration damping effect. Therefore, the total height of the quadrilateral phononic crystal double-layer beam structure constructed in this paper is 183 mm, the total width is 110 mm, and the total length is 550 mm, which means that five oscillators are placed vertically between the upper and lower beams, and five double-layer beam cells are placed horizontally periodically.

3. Numerical Results and Analysis

3.1. Energy Band Structure and Transmission Curves

The energy band structure diagrams of the ortho-two sided as well as ortho-quadrilateral vibrators are calculated using the finite element software COMSOL Mutiphysics. Figure 3a,c show the band structures of the ortho-quadrilateral and ortho-bipartite local oscillators, respectively, while Figure 3b,d present their corresponding displacement transmission curves. In order to verify the accuracy of the energy band structure diagrams, five bipartite vibrators as well as ortho-quadrilateral vibrators are arranged vertically according to the periodicity as shown in Figure 4a,b, for the finite-periodic resonator models shown in Figure 4, a vertical displacement excitation was applied at the bottom, and the displacement response was measured at the top. The excitation and response locations of the corresponding beam structures are indicated in Figure 1d. The vibration transmission curves of the two oscillators calculated using Equation (3) are shown in Figure 4a,b below, from which it can be seen that the transmission curve diagrams of the oscillators are basically the same as the width of the forbidden bandwidth calculated from the energy band structure diagrams, and both of them have opened a wider range of the bandgap, showing qualitative consistency between the band-structure predictions and the transmission responses. It is usually stipulated that the frequencies between 20 Hz and 200 Hz are low frequencies, so this paper mainly studies the frequencies below 200 Hz. From Figure 3a, the ortho-bipartite local oscillator exhibits two bandgaps at 50.2–87.9 Hz and 142.1–172.7 Hz, with a total bandwidth of 68.3 Hz. In contrast, the ortho-quadrilateral local oscillator exhibits three bandgaps below 200 Hz, with the first two located at 38.5–68.6 Hz and 82.3–103.4 Hz, respectively. The first bandgap of the ortho-quadrilateral oscillator starts at 38.5 Hz, which is lower than that of the ortho-bipartite oscillator at 50.2 Hz, indicating its ability to attenuate vibrations at lower frequencies. As shown in Figure 3b,d, the displacement transmission levels of the ortho-quadrilateral and ortho-bipartite local oscillators reach approximately −143 dB and −120 dB, respectively. The lower transmission level of the ortho-quadrilateral oscillator indicates stronger vibration attenuation at

the corresponding frequencies. The ortho-quadrilateral local oscillator has a lower first bandgap onset frequency and a more negative displacement transmission level than the ortho-bipartite local oscillator, indicating favorable low-frequency vibration attenuation characteristics. For comparison, Zhang et al. [22] reported two bandgaps at 60–70 Hz and 107–130 Hz for a pentagonal local resonator, with a total bandwidth of 33 Hz. In the present study, the quadrilateral local resonator exhibits its first two bandgaps at 38.5–68.6 Hz and 82.3–103.4 Hz, respectively. These results indicate that the quadrilateral configuration can also generate multiple low-frequency bandgaps, with the first bandgap starting at a lower frequency in the reported model. However, it should be noted that the lattice constants of the two models are 160 mm and 110 mm, and their other geometric parameters are not entirely identical. Therefore, the differences in bandgap characteristics cannot be attributed solely to the change in resonator configuration. Rather than establishing an unconditional performance advantage over the pentagonal structure, the present results demonstrate the bandgap characteristics of an alternative spatially connected resonator and provide an additional configuration for low-frequency vibration attenuation.

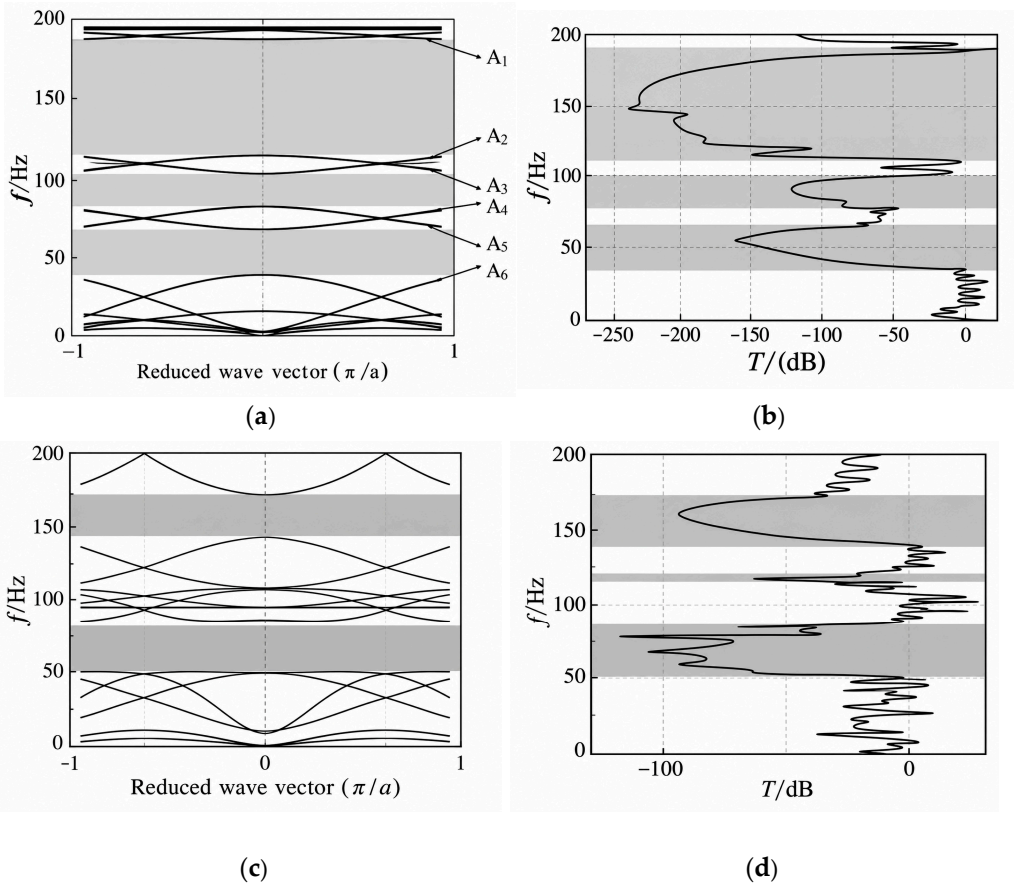

Figure 3. Band structures and displacement transmission levels calculated using COMSOL Multiphysics: (**a**) band structure of the ortho-quadrilateral local oscillator; (**b**) corresponding displacement transmission level; (**c**) band structure of the ortho-bipartite local oscillator; (**d**) corresponding displacement transmission level. The gray regions indicate the identified bandgap intervals, while the white regions represent frequency ranges outside the highlighted bandgaps.

In addition to the conventional band structure, the wave attenuation characteristics can also be explained using the complex band structure [7]. For the present local resonators, the imaginary part of the normalised Bloch wave vector, $\mathrm{Im}(k)a/2\pi$, is expected to exhibit nonzero values for evanescent modes within the bandgap regions, indicating exponential spatial attenuation, while the real part, $\mathrm{Re}(k)a/2\pi$, describes the corresponding phase varia-

tion. The detailed complex dispersion branches depend on the resonator configuration and propagation direction. Experimentally, the predicted vibration attenuation could be evaluated by applying harmonic excitation to a fabricated periodic structure and measuring the input and output vibration responses using accelerometers or laser Doppler vibrometry. The measured transmission responses could then be compared with the numerical predictions.

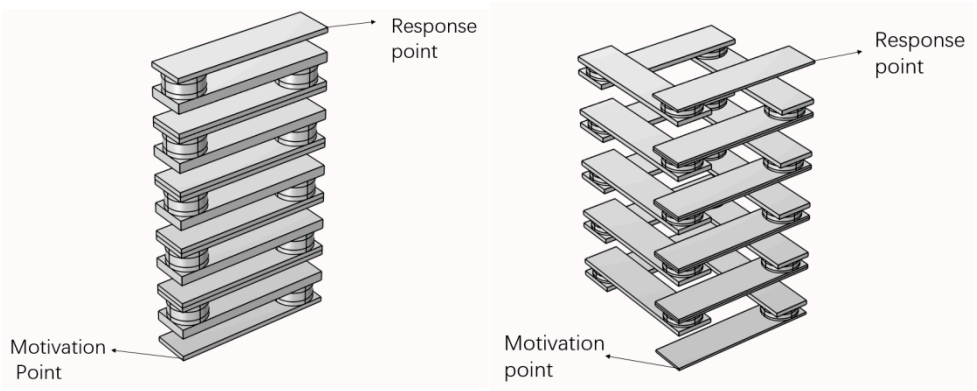

Figure 4. Schematic diagrams of the two phononic crystal beam configurations: (**a**) beam structure with a parallel arrangement of connecting plates; (**b**) beam structure with an orthogonal arrangement of connecting plates. The excitation and response points are indicated in each configuration.

3.2. Bandgap Characteristics of an Orthogonal Quadrilateral Oscillator

In order to better reveal the bandgap properties of the ortho-quadrilateral local-resonance-type phononic crystals, the displacement field corresponding to the eigenmode of the critical point as shown in the energy band structure diagram in Figure 2b is selected for the analysis, as shown in Figure 5.

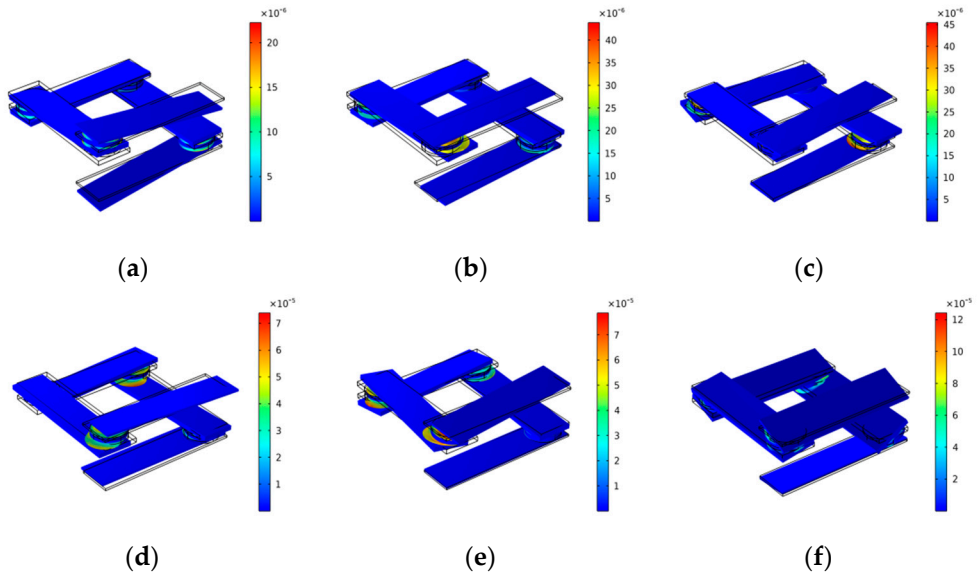

Figure 5. Displacement mode shapes of the ortho-quadrilateral local oscillator at six selected characteristic points (A1–A6) marked in the band structure in Figure 3a: (**a**) A1; (**b**) A2; (**c**) A3; (**d**) A4; (**e**) A5; (**f**) A6. The color scale represents the displacement magnitude, and the different mode shapes illustrate the translational and rotational vibrations of the connecting plates associated with local resonance.

In A1, the upper and lower side connecting plates are rotated along the yoz plane with the inter-plate portion as the axis, the left- and right-side connecting plates are rotated along the xoz plane with the inter-plate portion as the axis, the rear side connecting plate is rotated along the right multilayered cylinder in the xoy plane; in A2, the lowermost connecting plate is rotated along the yoz plane, the uppermost connecting plate, as well as the rear connecting plate, are rotated along the xoy plane with the intermediate portion as the axis, the left-side connecting plate undergoes translational movement along the xoy sheet, the bottom most connecting plate as well as the left most connecting plate undergoes translational movement along the xoy plane; in A3, the right-side connecting plate as well as the uppermost connecting plate undergoes torsion in the xoz plane as well as in the yoz plane, respectively, and the rear side connecting plate undergoes rotation along the right multilayered cylinder in the xoy plane, and the lower side connecting plate as well as the left-side connecting plate undergoes translation, the rear side connection plate rotates along the yoz plane with the intermediate part of the plate as the axis, the upper side connection plate and the right-side connection plate rotate along the xoz plane with the intermediate part of the plate as the axis; in A5, the uppermost connection plate and the rear side connection plate flip along the *y*-axis, the lowermost plate is basically static, the left-side plate rotates in the xoy plane, the right-side plate rotates in the xoz plane with the intermediate part of the plate as the axis; and in A6 the upper side connection plate and the rear side connection and the left and right-side connection plates rotate along the xoy plane. In A6, the upper side connection plate and the rear side connection and the left and right-side connection plates rotate along the *y*-axis and *x*-axis respectively, and the lower side connection is basically stationary. Observing the above modal diagrams, it can be found that the quadrilateral phononic crystal oscillator conforms to the characteristics of a spring-connected mass, in which the lead layer structure remains unchanged as the substrate, the rubber layer deforms to be the equivalent of a spring, and the connecting plate is the equivalent of a mass. The coupling of these modes produces such a wide multilayer bandgap of the ortho-quadrilateral oscillator below 200 Hz.

3.3. Energy Band Structure and Transmission Curves of Orthogonal Quadrilateral Vibrator Arrangement on a Single Beam

The five orthogonal quadrilateral local oscillators are periodically arranged in the vertical direction and then combined with the veneer to form a new cell, the new cell structure diagram is shown in the figure below, and the dimensional parameters and material parameters used in the calculation process are shown in Tables 1 and 2. The energy band structure calculated using the finite element software COMSOL Multiphysics is presented in Figure 6a. In order to verify the correctness of the energy band structure diagram, five new cells are periodically arranged in the transverse direction to form a new phononic crystal single-layer beam structure. An excitation point with initial displacement is applied to the bottom left of the single-layer beam structure, and an output point is added to the rightmost part of the single-layer beam structure, and its transmission curve is calculated by the software as shown in the figure below, and no significant opening of the forbidden band can be observed from the transmission curve, and the modal displacements of the six points in the energy band structure diagram are selected for analysis. The black regions in the band structure are formed by the overlap of numerous closely spaced, nearly flat dispersion branches, indicating a high density of vibration modes within these frequency ranges.

Observation of the modal displacement diagrams of the single beams and cells of the orthogonal quadrilateral localised vibrators reveals that the lower beams of modes B1, B3, and B5 mainly undergo translational motions in the plane and the rest of the vibrators remain basically stationary, the lower beams of mode B2 mainly undergo rotations along

the central axis and the rest of the vibrators remain basically stationary, and only one group of vibrators of modes B4 and B6 undergoes motions. From the above analysis of the modal diagrams at the critical points in the energy band structure diagram, it can be found that when the excitation point and the corresponding point are on the same side of the vibrator layer, the vibrators in the structure only have a very small number of individual vibrators to produce the effect of the part of the vibrator, which explains that the single-layer beams are unable to produce the bandgap. The generation of a bandgap is not simply a combination of superimposed vibrators, but requires a reasonable structural setup to generate a bandgap mechanism.

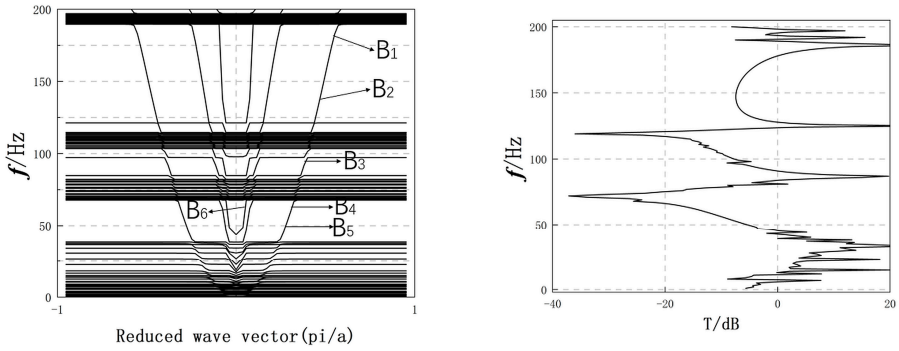

Figure 6. Band structure and displacement transmission level of the ortho-quadrilateral local oscillator single-layer beam calculated using COMSOL Multiphysics: (**a**) band structure; (**b**) corresponding displacement transmission level. The black regions in (**a**) represent densely clustered dispersion branches rather than bandgap regions.

3.4. Energy Band Structure and Transmission Curves of a Square Quadrilateral Vibrator Arrangement on a Double Beam

Similarly, five ortho-quadrilateral vibrators are arranged periodically in the vertical direction, and then an upper beam and a lower beam are added below each of them to form the ortho-quadrilateral phononic crystal double-layer beam structure, which is equivalent to one more upper beam than the single-layer beam structure, and the material and dimensional parameters used in the process of computation are as shown in Table 1 as well as Table 3. The energy band structure of the double-layer beam structure is computed using the finite element software COMSOL Mutiphysics, as shown in Figure 7a, and then an excitation point with initial displacement is applied at the same position, and the response point is added at the corresponding position. The energy band structure of the double-layer beam structure is calculated using the finite element software COMSOL Mutiphysics, as shown in Figure 7a, and the transmission curves of the double-layer beam structure are calculated as shown in Figure 7b, by applying an excitation point with an initial displacement at the same position and adding a response point at the corresponding position, as shown in Figure 1d. The open bandgap range of this double-layer beam structure is not found from the energy band structure diagram, but a wide forbidden band range is observed in the transmission curve diagram; in order to reveal the bandgap characteristics of the double-layer beam structure in this frequency band, the modal displacement diagram of the critical point in the energy band structure diagram of the double-layer beam structure is taken to continue the analysis, which is shown in Figure 8 below.

The corresponding vibration mode shapes are shown in Figure 9.

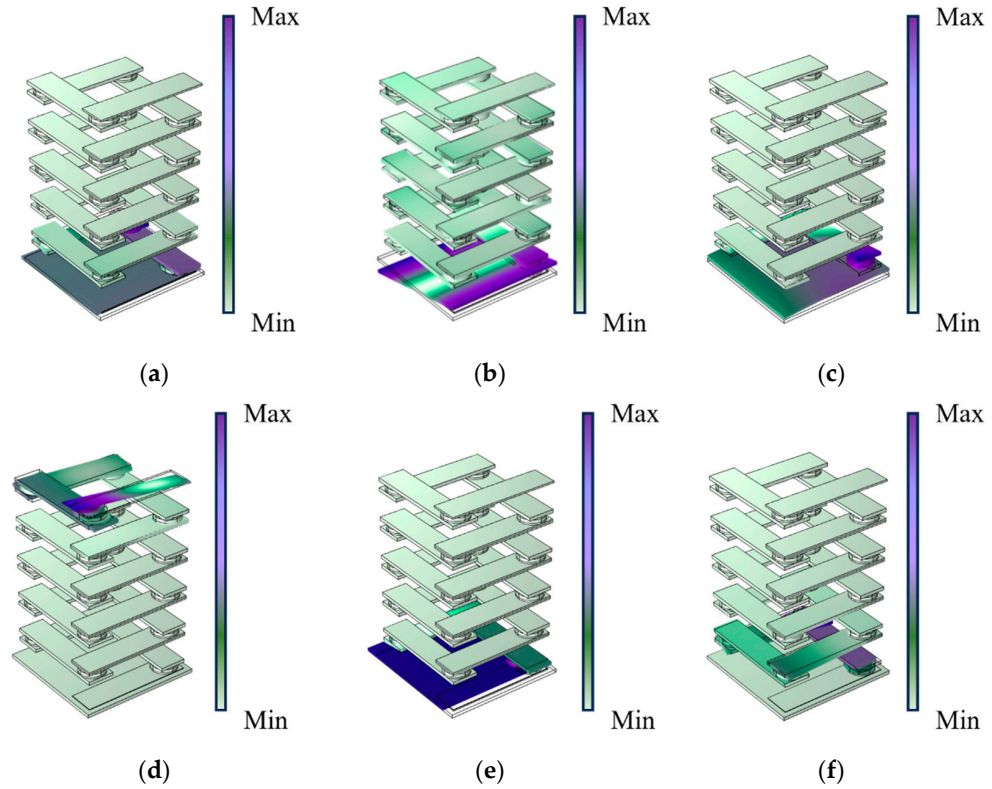

Figure 7. Displacement mode shapes of the ortho-quadrilateral local oscillator single-layer beam at six selected characteristic points (B1–B6) marked in the band structure in Figure 6a: (**a**) B1; (**b**) B2; (**c**) B3; (**d**) B4; (**e**) B5; (**f**) B6. The color scale represents the displacement magnitude. Modes B1, B2, B3, and B5 mainly involve the motion of the supporting beam, whereas modes B4 and B6 exhibit localised vibrations of the oscillators.

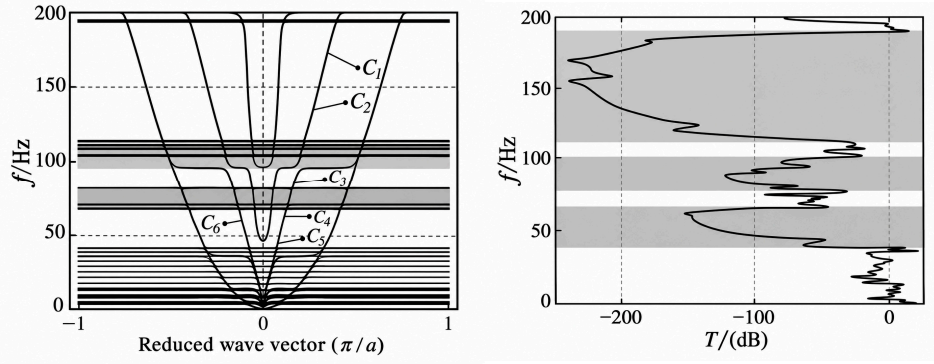

Figure 8. Band structure and displacement transmission level of the ortho-quadrilateral local oscillator double-layer beam calculated using COMSOL Multiphysics: (**a**) band structure; (**b**) corresponding displacement transmission level. The black regions in (**a**) represent densely clustered dispersion branches rather than bandgaps. The gray regions highlight selected frequency intervals for comparison with the transmission response, while the white regions indicate the remaining frequency ranges.

As shown in the above figure, the modal displacements at the critical point position in the energy band structure diagram of the double-layer beam with orthogonal localised oscillator are given. The upper and lower beams of the double-layer beam in modes C1, C5, and C6 are partially displaced along the plane, which can be coupled with the vibration of the bending elastic waves in the beam in the corresponding direction to form a bending elastic wave resonance bandgap. In modes C2, C3, and C4, the upper beams of the double-

layer beams torsionally move along the central axis, which is the result of mutual coupling with the bending vibration in the corresponding direction between the beams. By observing the above modal displacement diagrams, it can be found that no matter how the upper (lower) beams vibrate in these frequencies, the lower (upper) beams remain stationary, which proves that the vibration wave cannot be transmitted from one beam to another in these frequency bands, and further demonstrates that the double-layer beam structure possesses a better vibration damping effect. The reason why there is no obvious forbidden band in the energy band structure diagram but a wide range of forbidden bands in the transmission curve diagram is that the vibration in special frequency bands during the propagation of vibration in the middle of the upper and lower beams falls within the bandgap range of the quadrilateral local oscillator, which is the intrinsic damping interval of the quadrilateral oscillator, which enables the quadrilateral double-layer beam structure to open up such a wide range of bandgap.

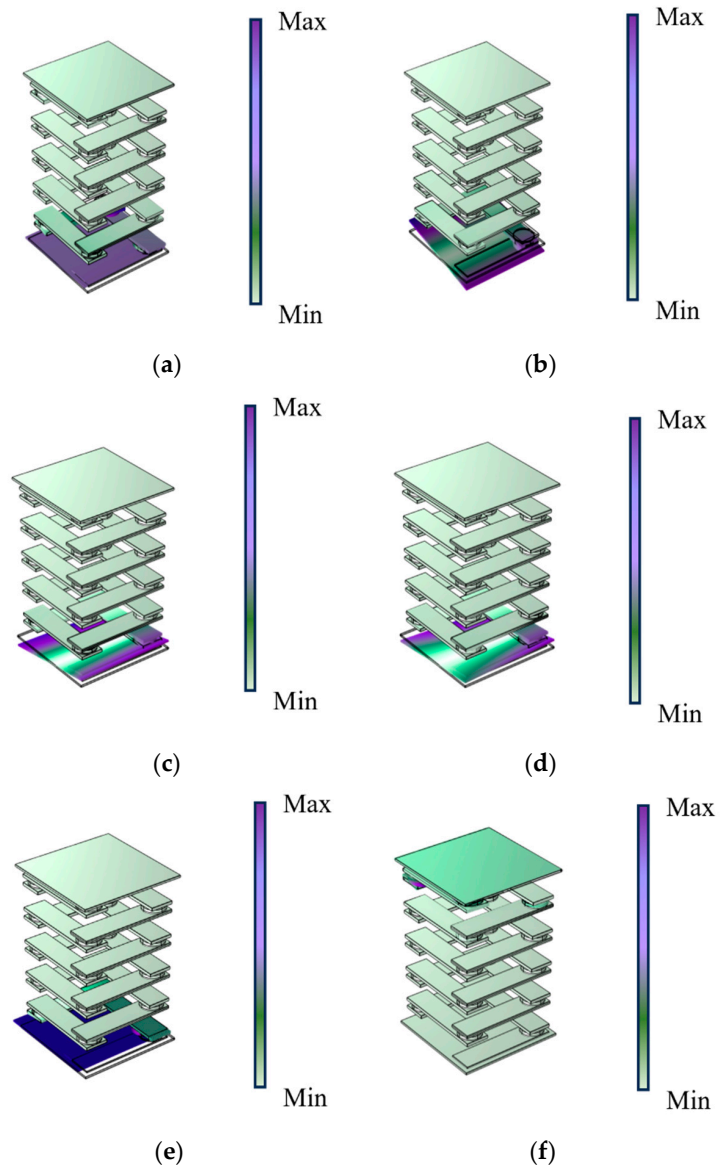

Figure 9. Displacement mode shapes of the ortho-quadrilateral local oscillator double-layer beam at six selected characteristic points (C1–C6) marked in the band structure in Figure 8a: (**a**) C1; (**b**) C2; (**c**) C3; (**d**) C4; (**e**) C5; (**f**) C6. The color scale represents the displacement magnitude. Modes C1, C5, and C6 mainly exhibit local displacement of the upper or lower beams, whereas modes C2, C3, and C4 involve torsional vibrations of the upper beam.

In order to have a clearer understanding of the damping characteristics of this double-layer beam structure, the vibration patterns of the double-layer beam structure under the action of frequencies within the intrinsic damping interval as well as frequencies outside the interval are selected as shown in Figure 10b, which shows that the vibration patterns of the double-layer beam are selected at a frequency of 5 Hz as well as at a frequency of 45 Hz. As can be seen from Figure 10b, when the frequency is outside the damping band of the double-layer beam, when the vibration occurs in one side of the beam, the other layer of the beam will also vibrate with it, and at this time, the double-layer beam does not have a damping effect; and when the frequency is within the damping band of the double-layer beam, as shown in Figure 10a, the upper layer of the beam will not be vibrated along with the vibration of the lower layer of the beam, which means that the vibration wave cannot be propagated between the double-layer beams at this frequency. This means that at this frequency, the vibration wave does not propagate between the double-layer beams, and the beams at this time have a better vibration isolation effect.

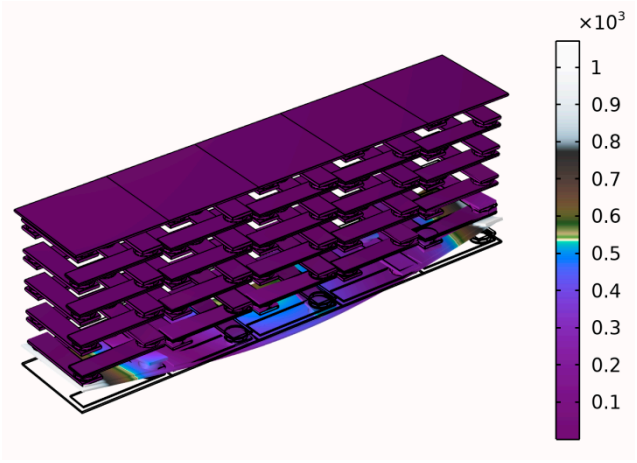

(**a**)

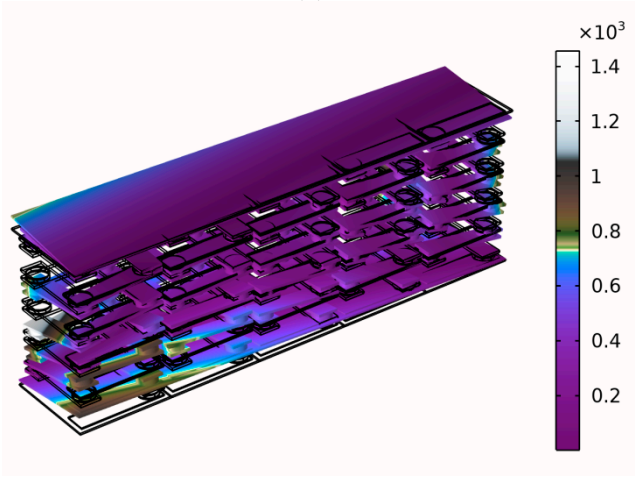

(**b**)

Figure 10. Vibration displacement distributions of the ortho-quadrilateral local oscillator double-layer beam at different excitation frequencies: (**a**) 45 Hz, within the vibration attenuation band; (**b**) 5 Hz, outside the vibration attenuation band.

3.5. Influence of Parameters on the Attenuation Band of Phononic Crystal Beam Structures

The dimensional and material parameters used in the calculations are shown in Tables 1 and 2. In order to investigate the effect of the choice of parameters on the vibration damping performance of the structure, the number of quadrilateral local oscillators between the beams, the radius of the multilayered cylinders, the thickness of the rubber

layer, the thickness of the lead layer, and the thickness and width of the upper and lower beams are chosen as variables to study the influence of these variables on the damping performance of the quadrilateral double-layer beams.

Three, four, and five ortho-quadrilateral localised vibrators are arranged uniformly and vertically between the beams to form a single-cell structure of ortho-quadrilateral localised vibrator double-layer beams, and then their transmission curves are calculated separately, as shown in Figure 11 below.

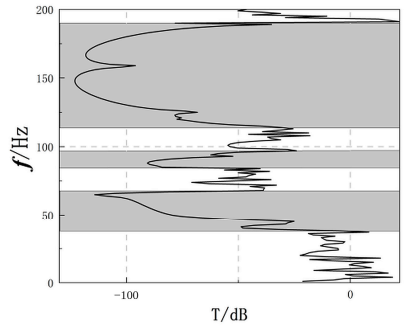

(**a**)

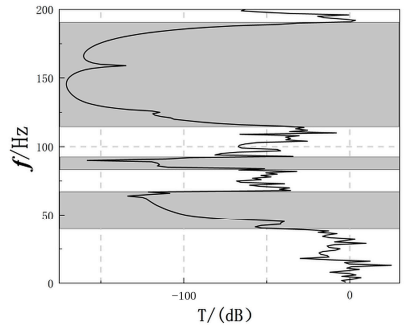

(**b**)

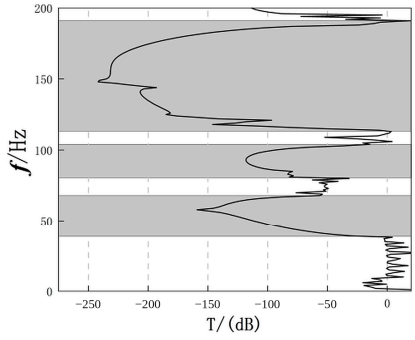

(**c**)

Figure 11. Displacement transmission levels of the ortho-quadrilateral local oscillator double-layer beam with different numbers of local oscillators: (**a**) three; (**b**) four; (**c**) five.

From the figure, it can be clearly seen that the total width of the bandgap does not change significantly with the increase in the number of orthogonal quadrilateral local oscillators arranged between the beams, but the loss value of vibration in the transmission process expands with the increase in the number of local oscillators, which proves that the vibration damping effect of the double-layer beams and the number of local oscillators between the beams of the double-layer beams as mentioned earlier are positively correlated.

Then, the multilayer cylinder radius, rubber layer thickness, lead layer thickness, as well as the thickness and width of the upper and lower beams of the single-layer beam of the ortho-quadrilateral phononic crystal are used as variables to study their effects on the structural bandgap characteristics, respectively, as shown in Figure 12.

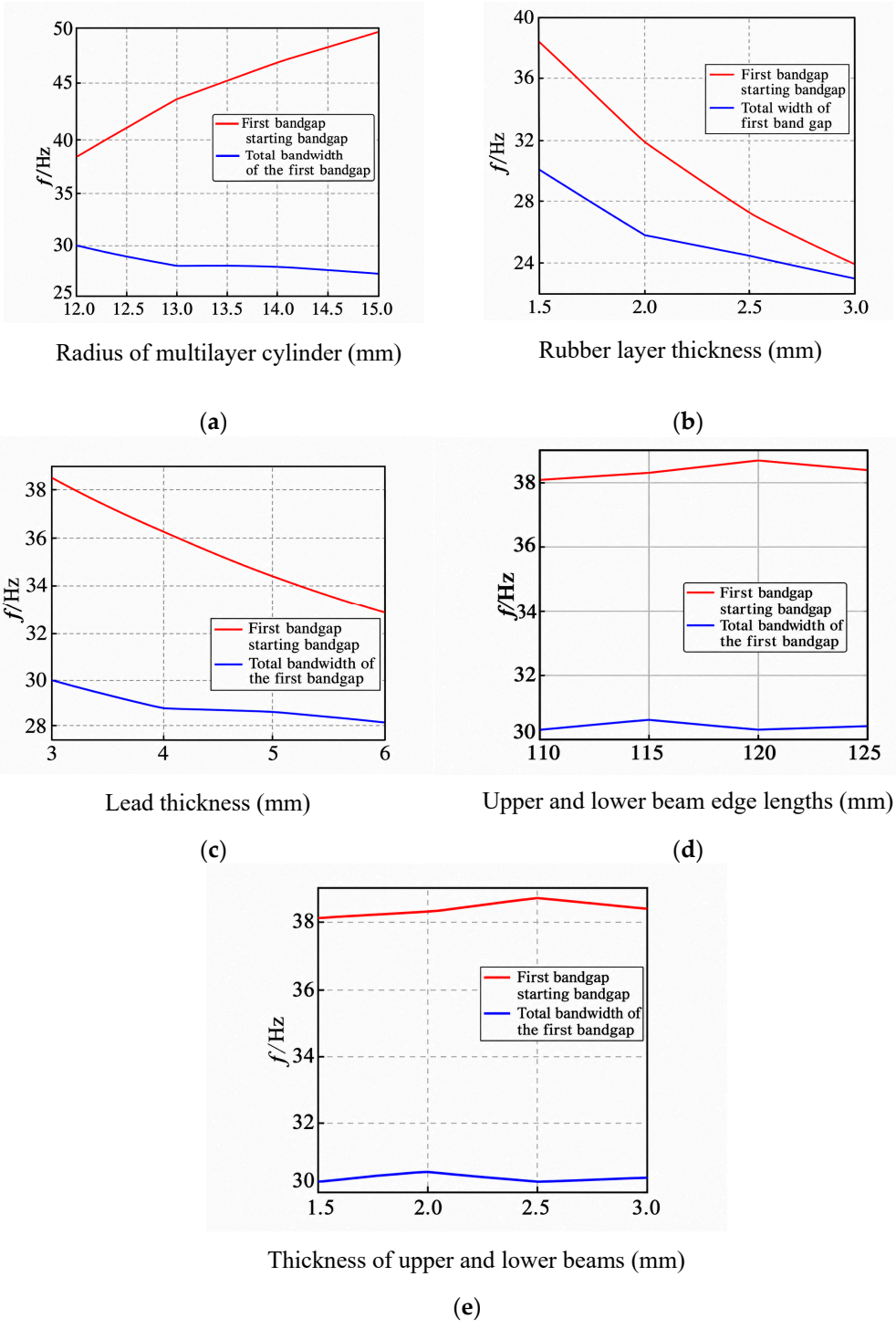

Figure 12. Effects of different geometric parameters on the first bandgap of the ortho-quadrilateral local oscillator double-layer beam: (**a**) radius of the multilayer cylinder; (**b**) rubber layer thickness; (**c**) lead layer thickness; (**d**) width of the upper and lower beams; (**e**) thickness of the upper and lower beams. The curves represent the numerical results obtained using COMSOL Multiphysics.

From the above figure, it can be concluded that with the increase in the radius of the multilayer cylinder, the first bandgap onset frequency of the double-layer beam has a larger

growth trend, and the total bandgap width of the first bandgap has a slight downward trend; with the increase in the thickness of the rubber layer, the onset frequency of the double-layer beam's first bandgap has a more obvious trend of decreasing, and the total bandgap width of the first bandgap has a downward trend, but the change relative to the onset frequency is relatively small; with the increase in the lead layer. With the increase in the lead layer, the onset frequency of the first bandgap of the double-layer beam and the total bandwidth of the first bandgap have an obvious decreasing trend; while the width and thickness of the upper and lower layers of the beams have less influence on the bandgap of the double-layer beam structure.

4. Conclusions

In this paper, a phononic crystal double-layer beam model with an ortho-quadrilateral local oscillator is investigated for low-frequency structural vibration attenuation. Firstly, the energy band structure diagrams and transmission curve diagrams of the oscillator structure are derived from finite element calculation methods and compared with the positive two-sided oscillator to study the bandgap characteristics of the oscillator. The energy band structure, transmission curve, and modal diagrams of the quadrilateral beam structure are then calculated and analysed to obtain the bandgap characteristics of the quadrilateral single-/double-layer beam. Finally, the effect of each parameter on the bandgap of the double-layer beam structure is investigated. It is summarised as follows:

1. The band structures and displacement transmission curves of the ortho-quadrilateral local oscillator were calculated using the finite element method. Three bandgaps were identified below 200 Hz, and pronounced vibration attenuation was observed within the corresponding frequency ranges. Compared with the ortho-bipartite local oscillator, the proposed configuration exhibits a lower first bandgap onset frequency and favorable low-frequency vibration attenuation characteristics.
2. The arrangement of quadrilateral vibrators on single-layer beams and double-layer beams is discussed, and the simulation is carried out by the finite element software, which results in the energy band structure diagrams, transmission curves, and modal diagrams. By analysing the modal diagrams of single-/double-layer beams at special points, it is concluded that the double-layer beams have a better vibration damping effect, while the single-layer beams have a relatively poorer effect. During the transmission of vibration between the beams of the double-layered beams, the orthogonal quadrilateral vibrator acts as a vibration isolator, attenuating and blocking the vibration waves whose frequencies are within its damping range.
3. The influence of material parameters on the bandgap of the double-layer beams is verified, in which the onset frequency of the first bandgap increases with the increase in the radius of the multilayer cylinder and the total bandgap of the first bandgap decreases; the onset frequency of the first bandgap and the total bandgap of the first bandgap decrease with the increase in the thicknesses of the rubber layer and the lead layer; and the thicknesses and widths of the upper and lower layers of the beams have little influence on the bandgap of the double-layer beams.

The proposed double-layer beam structure may provide a potential design for vibration isolation in shipboard equipment supports and marine machinery mounting structures, where low-frequency vibration transmission between connected structural members needs to be reduced. By adjusting the geometric parameters and the number of local oscillators, the vibration attenuation characteristics may be tailored to different frequency ranges, providing a reference for the design of low-frequency vibration control structures. It should be noted that the present study is based on numerical simulations of structural vibration, and

further experimental validation and acoustic analysis are required to evaluate its practical performance in shipboard applications.

Author Contributions: Software, H.Z.; investigation, H.Z.; writing—original draft preparation, H.Z.; supervision, Q.L.; writing—review and editing, Q.L.; methodology, D.Q.; project administration, D.Q.; funding acquisition, D.Q. All authors have read and agreed to the published version of the manuscript.

Funding: This research was funded by the National Natural Science Foundation of China grant number [52301373] and the Qinglan Project of Jiangsu Province of China.

Data Availability Statement: The original contributions presented in this study are included in the article. Further inquiries can be directed to the corresponding author.

Conflicts of Interest: The authors declare no conflict of interest.

References

1. Wen, X.; Hong, W.Q.; Yu, D.L. *Phononic Crystals*; National Defence Industry Press: Beijing, China, 2009.
2. Shu, H.; Li, S.; Dong, L.; Gao, E.; Zhang, F.; Gao, Y. A sonic crystal angular rod with ability of multi-dimensional and broadband vibration reduction. *Noise Control Eng. J.* **2013**, *61*, 55–69. [CrossRef]
3. Shu, H.; Liu, S.; Zhao, D.; Zhang, F.; Gao, E. A combined sonic crystal rod of Bragg type with ability of vibration reduction in broad frequency band. *Noise Control Eng. J.* **2012**, *60*, 42–61. [CrossRef]
4. Yu, D.L.; Liu, Y.Z.; Wang, G.; Weng, J.; Qiu, J. Longitudinal vibration band gap characteristics of one—Dimensional phononic crystal with rod structure. *Vib. Shock* **2006**, *25*, 104–106.
5. Kushwaha, M.S.; Halevi, P.; Dobrzynski, L.; Djafari-Rouhani, B. Acoustic band structure of periodic elastic composites. *Phys. Rev. Lett.* **1993**, *71*, 2022–2025. [CrossRef] [PubMed]
6. Martínez-Sala, R.; Sancho, J.; Sanchez, J.V.; Gomez, V.; Llinares, J.; Meseguer, F. Sound attenuation by sculpture. *Nature* **1995**, *378*, 241. [CrossRef]
7. Laude, V.; Achaoui, Y.; Benchabane, S.; Khelif, A. Evanescent Bloch waves and the complex band structure of phononic crystals. *Phys. Rev. B* **2009**, *80*, 092301. [CrossRef]
8. Röhlig, D.; Kuhn, E.; Teichert, F.; Thränhardt, A.; Blaudeck, T. Function phononic crystals. *EPL Europhys. Lett.* **2024**, *145*, ad1de9. [CrossRef]
9. Röhlig, D.; Thränhardt, A.; Laude, V.; Blaudeck, T. Giant band gaps in a phononic crystal with touching solid inclusions. *Phys. Rev. Appl.* **2025**, *23*, 054055. [CrossRef]
10. Röhlig, D.; Laude, V. Large band gaps in artificial crystals tuned by constriction shape. *Wave Motion* **2026**, *147*, 103785. [CrossRef]
11. Song, X.R.; Song, D.H.; Qi, Y. Studies on calculation method and bandgap properties of a nonlocal piezoelectric phononic crystal nanoplate. *Ferroelectrics* **2021**, *57*, 132–144. [CrossRef]
12. Jin, J.; Hu, N.D.; Hu, H.P. Investigation of size effect on band structure of 2D nano-scale phononic crystal based on nonlocal strain gradient theory. *Int. J. Mech. Sci.* **2022**, *219*, 107100. [CrossRef]
13. Chen, M.D.; Wang, N.; Xiao, H. Application of Piezoelectric Materials in Traditional Sound Absorption Structures. *Mater. Rep.* **2023**, *37*, 22010070.
14. Hhuang, K.C.; Yuan, Z.W.; Guo, Y.Q.; Lv, X.F. Extracting torsional bandgaps and transient waves in phononic crystal beams: Method and validation. *J. Sound Vib.* **2020**, *467*, 115004. [CrossRef]
15. Jiang, S.; Dai, L.X.; Chen, H.; Hu, H.P.; Jiang, W.; Chen, X.D. Folding beam-type piezoelectric phononic crystal with low-frequency and broad bandgap. *Appl. Math. Mech.* **2017**, *38*, 411–422. [CrossRef]
16. Oudich, M.; Li, Y.; Assouar, B.M.; Hou, Z. A sonic bandgap based on the locally resonant phononic plates with stubs. *New J. Phys.* **2010**, *12*, 083049. [CrossRef]
17. Yang, K.; Tang, Y.; Wu, H.L.; Wang, B. Research on the low-frequency sound insulation properties of membrane-type local resonant phononic crystals. *Ship Sci. Technol.* **2022**, *44*, 26–29.
18. Guo, X.; Guo, H.Y.; Hong, M. Research on vibration and noise reduction of local resonant phononic crystal plate. *J. Ship Mech.* **2021**, *25*, 509–516.
19. Li, Z.Y.; Zheng, Y.Z.; Ma, T.X.; Zhang, C. Smart piezoelectric phononic crystals and metamaterials: State-of-the-art review and outlook. *Chin. Sci. Bull.* **2022**, *67*, 1305–1325. [CrossRef]
20. Zhang, X.; Liu, Z.; Li, C.; Xiao, X.; Wang, H. Investigation of low-frequency sound insulation performance of high-speed train profile structure with gyro-type phononic crystal. *Noise Vib. Control* **2022**, *42*, 220–226.
21. Kang, T.; Sun, X.; Song, T.; Sun, W.; Liao, T.; Tan, Z. Low-frequency bandgap characteristics and formation mechanism of two-dimensional hollow scatterer phononic crystal plates. *J. Acoust.* **2020**, *45*, 601–608.

22. Zhang, S.K.; Qian, D.H.; Zhang, Z.W.; Ge, H.R. Low-Frequency Bandgap Characterization of a Locally Resonant Pentagonal Phononic Crystal Beam Structure. *Materials* **2024**, *17*, 1702. [CrossRef] [PubMed]
23. Yu, D.; Liu, Y.; Wang, G.; Wen, J.; Qiu, J. Torsional vibration bandgap study of one-dimensional rod-like structure phononic crystals. *Vib. Shock* **2006**, *25*, 104–106.
24. Shen, C.; Huang, J.; Chen, M.; Qian, D.; Wang, J.; Zhuang, J. Study of bandgap characteristics of phononic crystal double-layer beam structure based on multilayer S-shaped local oscillators. *Vib. Shock* **2023**, *42*, 197–204.
25. Qian, D.H.; Shi, Z.Y.; Wu, J.H. Bandgap properties in stubbed-on locally resonant phononic crystal Bandgap properties in stubbed-on locally resonant phononic crystal double panel structures. *J. Vib. Meas. Diagn.* **2019**, *39*, 484–494.
26. Placidi, L.; El Sherbiny, M.G.; Baragatti, P. Experimental investigation for the existence of frequency band gap in a microstructure model. *Math. Mech. Complex Syst.* **2022**, *9*, 413–421. [CrossRef]
27. Boutin, C.; D'ANnibale, F.; Pancella, C.; Giorgio, I. On the mechanical behavior of elastic crenelated beams. *J. Appl. Mech.* **2026**, *93*, 091004. [CrossRef]
28. Camley, R.E.; Djafari-Rouhani, B.; Dobrzynski, L.; Maradudin, A.A. Transverse Elastic Waves in Periodically Layered Infinite, Semi-Infinite, and Slab Media. *J. Vac. Sci. Technol. B Microelectron. Nanometer Struct.* **1982**, *1*, 371–375. [CrossRef]
29. Gao, G.Q.; Ma, S.L.; Jin, F.; Kim, T.B.; Lu, T.J. Forbidden band properties of acoustic waves in two-dimensional solid/fluid phononic crystals. *Phys. Lett.* **2010**, *59*, 393–400.
30. Qiu, C.; Liu, Z.; Mei, J.; Ke, M. The Layer Multiple-Scattering Method for Calculating Transmission. *Solid State Commun.* **2005**, *134*, 765–770. [CrossRef]

Disclaimer/Publisher's Note: The statements, opinions and data contained in all publications are solely those of the individual author(s) and contributor(s) and not of MDPI and/or the editor(s). MDPI and/or the editor(s) disclaim responsibility for any injury to people or property resulting from any ideas, methods, instructions or products referred to in the content.